Fluorophore Binding Aptamers as a Tool for RNA Visualization

Katja Eydeler, Eileen Magbanua, Arne Werner, Patrick Ziegelmüller, and Ulrich Hahn*
Department of Chemistry, Institute of Biochemistry and Molecular Biology, University of Hamburg, 20146 Hamburg, Germany

ABSTRACT Fluorescence correlation spectroscopy (FCS) is suitable for the detection of fluorescent molecules in living cells. For the visualization of mRNA, we genetically fused a fluorophore-specific RNA aptamer to the coding mRNA of the green fluorescent protein, as well as to noncoding sequences. Using these constructs, we showed that the aptamer portion of the mRNA still binds the fluorophore in the nanomolar range as determined via FCS. Furthermore, the binding took place in the context of total RNA extract. A tandem construct of the RNA aptamer even exhibited a lower K_d than the monomer. This FCS-based method establishes a tool for minimal invasive detection of RNA at the single molecule level in individual living cells.

INTRODUCTION

The localization and investigation of endogenous mRNAs in living cells is an important tool, because the subcellular localization of mRNA plays a key role in the regulation of different processes like morphogenesis, cell migration, and memory formation (1–3). Because there is no RNA molecule known with an intrinsic fluorescence like green fluorescent protein (GFP) for proteins, indirect methods have been used to analyze the localization of RNA transcripts in living cells. With the help of molecular beacons (4–6) or fluorescently labeled mRNA (7–9), different RNAs could be visualized in living cells and oocytes. Fluorescent proteins fused to RNA binding proteins like MS2 coat protein (10,11), PUMILIO1 (12), or RNA aptamer-binding proteins (13) were used to tag mRNA, allowing for real-time imaging in bacteria, yeast, and human cells. For the study of the subcellular localization, transport, metabolism of RNA, and interactions of RNA molecules with other components, e.g., in RNA interference, the relative size of the protein tags is enormous and adds up to 27–270 kDa for a single GFP protein and the MS2 coat protein tag, respectively. A reduction of size for the tag would be achieved by using fluorophore binding aptamers (14), which weigh <2 kDa. The aptamer SRB2m binds the fluorophore sulforhodamine B with high specificity and affinity (15). Interactions of aptamers with their fluorescent target can be monitored via fluorescence correlation spectroscopy (FCS) (16), and this method is capable of detecting down to ~40 nM RNA in real time (17). FCS analysis showed an increase in diffusion time of sulforhodamine B on binding to SRB2m (A. Werner, unpublished data). Therefore, SRB2m seems to be suitable for monitoring RNA dynamics at the single molecule level.

The aim of this work was to further investigate the potential applications of the RNA aptamer SRB2m for fluorescent labeling of RNA. Different fusion constructs of the aptamer were produced by in vitro transcription and analyzed by FCS. The fusion constructs of SRB2m with vector-derived noncoding RNA or enhanced green fluorescent protein (EGFP)-coding mRNA still bind their target, sulforhodamine B. Even in the presence of total RNA from mammalian cells, binding was retained.

MATERIALS AND METHODS

Plasmid constructs

Synthetic DNA of SRB2m, including a T7 promoter, was used as a template for polymerase chain reaction (PCR) amplification. Corresponding restriction sites were introduced with primer Pf *Eco*RI (5′ CCATGAATTCGGA ACCTCGCTTCGGCG 3′) and Pr *Not*I (5′ GTTAACCGCCTCAGGTTCC GCGGCCGCATGG 3′) with subsequent cloning of the PCR product into pcDNA3.1(+) (Invitrogen, Karlsruhe, Germany). For the tandem SRB2m construct, SRB2m was provided with a short linker and adjacent restriction sites using the primer Pf *Bam*HI (5′ CCATGGATCCGGAACCTCGCTTC GGCG 3′), Pr *Eco*RI long (5′ CCATGAATTCCCGAGCTCGGATAAAAA AAAAAGGAACCTGAGGCGGTTAAC 3′), and Pr *Eco*RI short (5′ CCAT GAATTCCCGAGCTCGGAT 3′). The PCR product was then cloned into pcDNA3.1-SRB2m to produce a tandem orientation of SRB2m with a linker sequence in between (5′ TTTTTTTTTTATCCGAGCTCGG 3′) to allow proper folding of the aptamer. For construction of pcDNA3.1-EGFP-SRB2m, EGFP was excised from pEGFP-N1 (Clontech, Heidelberg, Germany) by *Pst*I and *Not*I and cloned into pUC18 (Fermentas, St. Leon-Rot, Germany). To eliminate a *Cfr*9I restriction site in pUC18-EGFP, a *Pae*I/*Bsh*TI restriction was carried out. Resulting overhangs were degraded by mung bean nuclease before blunt end ligation. The SRB2m gene insert was generated by four complementary oligonucleotides (5′ CCGGGGGAA CCTCGCTTCGGCGATGATG 3′, 5′ GAGAGGCGCAAGGTTAACCG CCTCAGGTCCG 3′, 5′ CCCTTGGAGCGAAGCCGCTACTACCTCTCC GCGTTCCA 3′, and 5′ ATTGGCGGAGTCAAGCTTAA 3′) that were assembled into the SRB2m gene with flanking *Cfr*9I and *Eco*RI restriction sites to allow cloning in the 3′ UTR of EGFP in pUC18-EGFP. The resulting EGFP-SRB2m insert was cloned into pcDNA3.1(+) using *Hind*III and *Eco*RI restriction sites. All constructs were verified by DNA sequencing.

T7 transcription and purification of RNA

RNA was transcribed in vitro with T7 RNA polymerase. After *DNase*I treatment, transcripts smaller than 1000 nt were purified on a denaturing 8 M urea 8% polyacrylamide gel or with Micro Bio-Spin P30 columns (Biorad, Munich, Germany) if only the expected transcripts were obtained. T7 transcripts

Submitted December 1, 2008, and accepted for publication January 23, 2009.

*Correspondence: uli.hahn@uni-hamburg.de

Editor: Samuel Butcher.

0006-3495/09/05/3703/5 $2.00

doi: 10.1016/j.bpj.2009.01.041

larger than 1000 nt were purified on a 2% formaldehyde agarose gel. DNA templates for the in vitro synthesis of the aptamer fusion constructs were generated either by PCR with the primer Pf T7 (5′ TCTAATACGACTCAC TATAGG 3′) and Pr BGH (5′ CATTTTATTAGGAAAGGACAG 3′) or by linearizing pcDNA3.1-SRB2m with *Not*I or pcDNA3.1-EGFP-SRB2m with *Eco*147I (1395 bp downstream of SRB2m). Folding of the RNA was done in 10 mM NaHepes pH 7.4, 100 mM KCl by heating to 70°C for 10 min, followed by cooling down on ice for 30 s with the addition of 5 mM $MgCl_2$. Finally, the samples were incubated 1 h at room temperature and centrifuged 14,000 × *g* to remove possible aggregates.

Secondary structure analysis

Secondary structure of RNAs were analyzed by Mfold (18,19).

FCS

The principle of FCS is the detection of fluorescence intensity fluctuations $\delta F(t)$ in a well-defined femtoliter-sized confocal detection volume (20,21). The fluctuations are induced by fluorescent particles diffusing in and out of the detection volume because of Brownian motion. The temporal autocorrelation function is the correlation of a time series with itself shifted by time τ, as a function of τ:

$$G(\tau) = \frac{\langle \delta \mathrm{I}(t)\delta \mathrm{I}(t+\tau)\rangle}{\langle \mathrm{I}(t)\rangle^2}, \quad (1)$$

where $\mathrm{I}(t+\tau)$ is the fluorescence intensity in single photon counting method obtained from the detection volume at delay time τ. The residence time τ_D (τ_{Diff}) of the fluorescent particle in the detection volume is defined at the deflection point of the correlation function. Different diffusion species can be distinguished if their masses differ with a factor of 8 or more because $\tau_{Diff} \approx \sqrt[3]{m}$. By using the LSM 5 software (Zeiss, Jena, Germany), the autocorrelation data were fitted to the Levenberg-Marquardt algorithm assuming free three-dimensional diffusion and considering triplet excited state (22):

$$G(\tau) = 1 + \frac{1}{N} \times \left(\frac{1 - T + Te^{-\frac{\tau}{\tau_T}}}{1-T}\right) \times \left\{\sum_{i=1}^{n} \frac{f_{,i}}{\left(1+\frac{\tau}{\tau_{Diff,i}}\right)\sqrt{1+\frac{\tau}{\tau_{Diff,i}}S^{-2}}}\right\}. \quad (2)$$

The validity of the measurements was proven by a χ^2 test and the residual deviations of the fit. The optical setup was examined using the standard fluorophore Rhodamine 6 Green ($D_i = 2.8 \times 10^{-10}$ m^2 s^{-1}) with

$$D_i = \frac{\omega_1^2}{4 \times \tau_{Diff}}, \quad (3)$$

where ω_1 represents half of the short axis of the volume element and was set to be 198 nm. With ω_2 corresponding to half of the long axis of the volume, the effective volume is

$$V_{eff} = \omega_1^2 \times 2 \times \pi \times \omega_2 = 2 \times \pi \times S \times \omega_1^3. \quad (4)$$

The structure parameter S was determined to be 5.5, so the approximate size of V_{eff} was ~0.3 fl. With the number of fluorescent particles in the detection volume, N, the concentration $[N]$ can be calculated using

$$[N] = \frac{N}{N_A \times V_{eff}}, \quad (5)$$

with $N_A = 6.022 \times 10^{23}$ mol^{-1}. With the help of the Stokes-Einstein equation, the hydrodynamic radius r_H can be calculated as

$$r_H = \frac{k \times T}{6 \times \pi \times \eta_V \times D_i}, \quad (6)$$

with k being the Boltzmann constant, η_V being the viscosity (1.002×10^{-3} kg m^{-1} s^{-1}) of the solution, T being the temperature, and D_i being the diffusion coefficient. In binding processes, the complex fraction Y is defined as $Y = [C]/[A] + [C]$, with C as the complex and A as the unbound ligand. Changes of the molecular brightness, η, during binding processes have to be accounted for (23):

$$Y' = \frac{Y \times \eta_C^2}{(1-Y) \times \eta_A^2 + Y \times \eta_C^2}. \quad (7)$$

All experiments were carried out at room temperature. For titration experiments, the sample volume was 20 or 40 μL. According amounts of RNA stock solution (10 mM NaHepes pH 7.4, 100 mM KCl, and 5 mM $MgCl_2$) were added to a 13-nM sulforhodamine B solution, (10 mM NaHepes pH 7.4, 100 mM KCl, 5 mM $MgCl_2$), followed by 1 min incubation. The data were collected 10 times for 30 s in each titration step. Three to four independent experiments were done. The K_d-values were calculated using GraphPad Prism 4.03 (GraphPad Software, San Diego, CA). For binding assays of total RNA from COS-7 cells, RNA was prepared and sulforhodamine B solution was added to a final concentration of 13 nM.

Cell culture and preparation of total RNA

COS-7 cells were cultivated in Dulbecco's modified Eagle medium (DMEM) without phenol red, containing 10% fetal bovine serum, 100 U/mL penicillin G, 100 mg/mL streptomycin, and 4 mM L-glutamine. The cells were transfected with plasmid DNA using Lipofectamine (Invitrogen). The total RNA was prepared 2 days after transfection using the RNeasy MiniKit (Qiagen, Hilden, Germany).

Reverse transcription-PCR and gel electrophoresis

Before reverse transcription-PCR (RT-PCR), the sample was treated with DNase I. For RT-PCR, first-strand cDNA was synthesized with 200 U of RevertAid M-MuLV Reverse Transcriptase using 5 μg total RNA from COS-7 cells and the primer Pr SRB2m (5′ GGAACCTGAGGCGGTTAAC 3′). Double-stranded DNA was generated by PCR amplification with Taq Polymerase and the primers forward (5′ TCTAATACGACTCACTATAGG 3′) and reverse (5′ GGAACCTGAGGCGGTTAAC 3′). Products were analyzed on 10% polyacrylamide gels in Tris-borate buffer. All enzymes were purchased from Fermentas.

RESULTS AND DISCUSSION

To examine the binding properties of the elongated sulforhodamine B binding aptamer SRB2m, the aptamer-coding oligonucleotide was cloned into the vector pcDNA3.1(+) and different fusion constructs of vector-encoded RNA and the aptamer were produced by T7 transcription. To produce a dimer arrangement of the aptamer, a tandem repeat was cloned into the vector and transcribed. In addition, different fusion constructs were produced by PCR (Fig. 1). Despite the extension of the SRB2m-sequence, the secondary structures of these constructs still exhibited folding into the SRB2m structure, as predicted using Mfold (18). To determine the binding properties of the fusion constructs to sulforhodamine B, the diffusion times of the dye in complex with

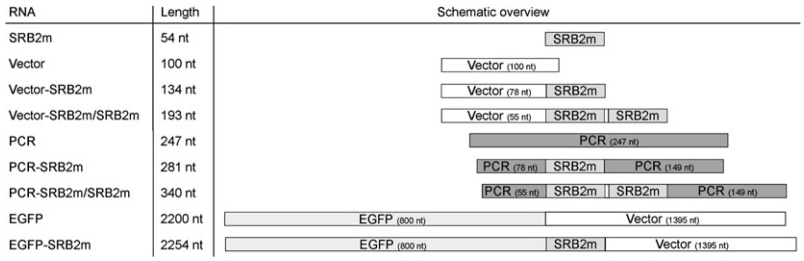

FIGURE 1 Schematic representation of different RNAs produced by in vitro T7 transcription. Individual SRB2m, fusion constructs of SRB2m with different vector sequences, EGFP-coding mRNA, and corresponding controls without SRB2m were used in this study.

the different RNAs were derived through FCS titration experiments using a model for one diffusion species (22). The diffusion time of sulforhodamine B ($\tau_{Diff} = 30.0 \pm 1.5$ μs) increased up to $\tau_{Diff} > 300$ μs after addition of RNA (Fig. 2), implying binding of the fluorophore to the aptamer portion of the different RNAs. Saturation was achieved at an RNA concentration of 2–3 μM. The individual SRB2m RNA without flanking sequences elevated the diffusion time to $\tau_{Diff} = 120$ μs. Control RNA without the aptamer did not lead to an increase of diffusion time. These data conclude a specific binding of sulforhodamine B to the aptamer SRB2m even in the presence of up to 227 nucleotides flanking RNA sequences.

To calculate the proportion of the different sulforhodamine B-SRB2m complexes, a fitting model for two different species was used (22) in which the diffusion time of the free fluorophore was fixed to ~30 μs and changes of molecular brightness during the titration (from ~20 kHz to ~40 kHz) were considered (23). K_d values in the nanomolar range of the fluorophore in complex with the elongated aptamer were obtained (Table 1). These values are in accordance with published data for the aptamer SRB2m of 310 nM $\pm$ 60 nM, 70 nM $\pm$ 10 nM, and 238 $\pm$ 24 nM, which were obtained from fluorescence anisotropy, affinity chromatography (15), and FCS analysis (A. Werner, unpublished data), respectively. Tandem repeats of the aptamer in the fusion constructs resulted in stronger binding to the fluorophore with K_d values of 70 $\pm$ 5 nM and 62 $\pm$ 6 nM compared with K_d values of 120 $\pm$ 17 nM and 630 $\pm$ 60 nM for the monomer fusion constructs. The diffusion coefficients, D, and hydrodynamic radii, r_h, were calculated from the determined diffusion times at saturation (Table 1). These values correspond to the theoretically calculated data and are comparable to experimental data using other RNA molecules, e.g., 5S rRNA (120 nt) with $D = 5.9 \times 10^{-11}$ m^2/s and $r_h = 3.6 \times 10^{-9}$ m (24).

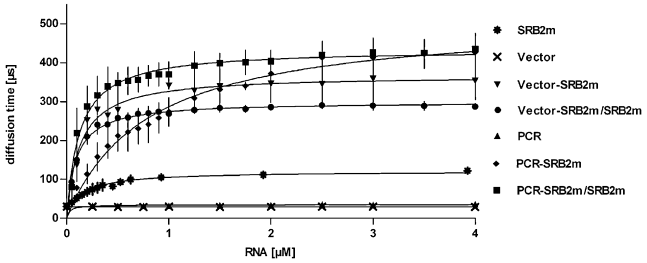

FIGURE 2 Binding of sulforhodamine B to SRB2m-constructs analyzed with FCS. Diffusion times, τ_{Diff}, of sulforhodamine B in complex with various SRB2m-constructs and concentrations were determined. To ensure proper folding of SRB2m constructs, RNA was denatured by heat and refolded. Values depicted represent the average of at least three independent measurements (mean $\pm$ SD, $n \geq 3$) with a measurement period of 10 $\times$ 30 s.

For in vivo applications, the specific binding of sulforhodamine B to SRB2m was tested in the presence of total RNA extract. For this purpose, total RNA of COS-7 cells transfected with the vector pcDNA3.1(+) containing the SRB2m aptamer gene was isolated and examined for binding of the fluorophore via FCS. After the addition of isolated total RNA extract to sulforhodamine B, the diffusion time of fluorescent particles increase from $\tau_{Diff} = 34$ μs to 384 μs $\pm$ 296 μs, indicating the formation of an RNA-fluorophore-complex (Fig. 3). In contrast, RNA from pcDNA3.1(+) transfected control cells did not increase the diffusion time, indicating that the fluorophore binds specifically to SRB2m even in the presence of total RNA extract. The presence of the aptamer-RNA in the isolated total RNA extract was further proved by RT-PCR, showing a product length of 150 bp and no product for control cells (Fig. 4).

A requirement for the detection of RNA molecules in vivo using fluorophores is the binding of sulforhodamine B to SRB2m-mRNA constructs. Therefore, SRB2m was fused to the 3′ UTR of the EGFP coding mRNA. At the in vitro transcription, an additional 1395 nucleotides of the vector were transcribed downstream of the SRB2m sequence (Fig. 1). Binding of sulforhodamine B to this EGFP-SRB2m construct was again detected through analysis of the diffusion time of sulforhodamine B via FCS. Increasing concentration of EGFP-SRB2m mRNA caused a rise of diffusion time of

TABLE 1 Determined dissociation constants K_d, diffusion coefficients D, hydrodynamic radii r_h, and diffusion times τ_{Diff} of the sulforhodamine B in complex with SRB2m RNA fusion constructs

	Determined values			
	K_d [nM]	D [m^2/s]	r_h [m]	τ_{Diff} [μs]
SRB2m	238 $\pm$ 24	7.3 $\times$ 10^{-11}	2.9 $\times$ 10^{-9}	122 $\pm$ 3.0
Vector-SRB2m	120.6 $\pm$ 17.5	2.75 $\times$ 10^{-11}	7.80 $\times$ 10^{-9}	357 $\pm$ 52.1
Vector-SRB2m/SRB2m	70.5 $\pm$ 4.9	3.38 $\times$ 10^{-11}	6.34 $\times$ 10^{-9}	290 $\pm$ 9.5
PCR-SRB2m	629.3 $\pm$ 62.3	2.307 $\times$ 10^{-11}	9.31 $\times$ 10^{-9}	426 $\pm$ 43.2
PCR-SRB2m/SRB2m	62.4 $\pm$ 5.6	2.23 $\times$ 0^{-11}	9.62 $\times$ 10^{-9}	440 $\pm$ 45.4

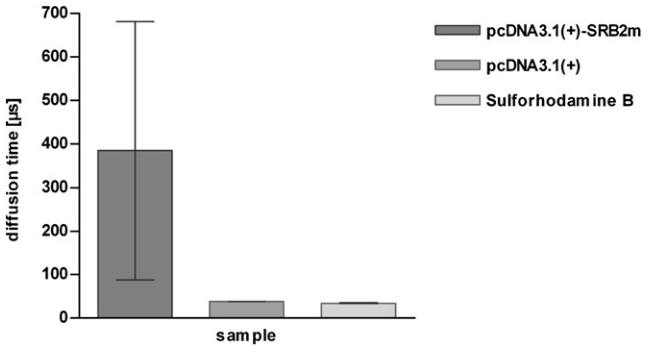

FIGURE 3 Binding of sulforhodamine B to in vivo transcribed SRB2m in the presence of total RNA extract. Total RNA (800 ng/μL) from COS-7 cells, transfected with pcDNA3.1-SRB2m or pcDNA3.1(+) without aptamer gene, was isolated. The binding of sulforhodamine B to the RNA was determined by monitoring the diffusion time with FCS.

sulforhodamine B, indicating formation of a complex consisting of fluorophore and mRNA (Fig. 5). The diffusion time, τ_{Diff}, of fluorescing particles increased from ~30 μs (sulforhodamine B without RNA) to >3000 μs for the complex of sulforhodamine B with EGFP-SRB2m. As a negative control, mRNA without SRB2m (Fig. 1) showed no change in diffusion time. With increasing amounts of SRB2m-mRNA, up to 50% of sulforhodamine B was bound by the EGFP-SRB2m mRNA. In contrast, no fluorophore was bound by the negative control RNA. However, a K_d of 1.13 μM could be calculated for the binding of sulforhodamine B to EGFP-SRB2m

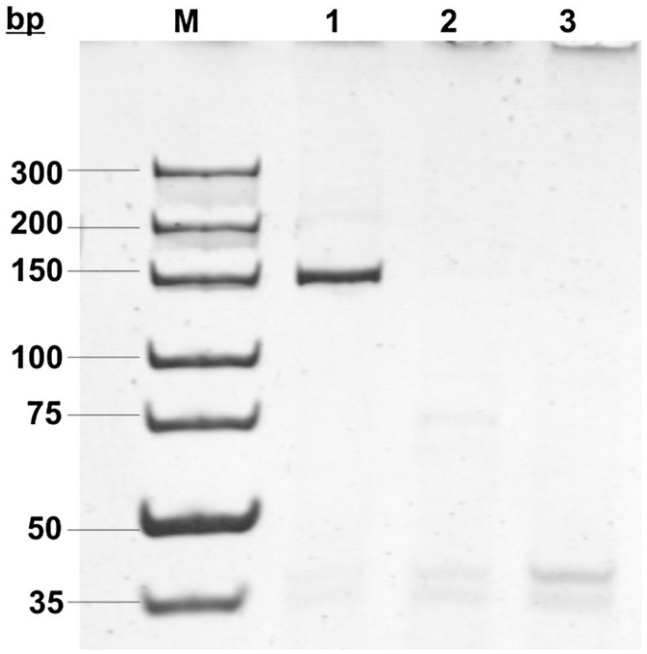

FIGURE 4 Analysis of aptamer transcription by RT-PCR (*1*). The transcription of SRB2m in COS-7 cells transfected with pcDNA3.1-SRB2m was proven by RT-PCR (*2*). COS-7 cells transfected with pcDNA3.1-SRB2m without RT (*3*), RT-PCR of COS-7 cells transfected with pcDNA3.1(+).

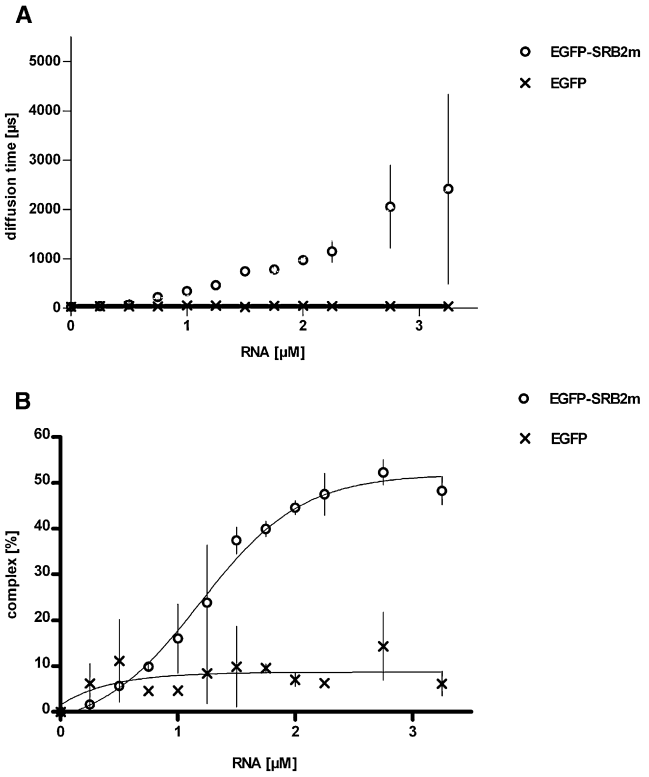

FIGURE 5 Binding of sulforhodamine B to EGFP-SRB2m mRNA analyzed by FCS. Diffusion times, (*A*) τ_{Diff}, and (*B*) percentage of complex formation were determined. Values depicted represent the average of two independent measurements (mean $\pm$ SD, $n = 2$) with a measurement period of 10 $\times$ 30 s.

mRNA. Only 50% of the bound fluorophore contributed to the emission signal. The unexpected high dissociation constant of 1.13 μM for the EGFP-SRB2m mRNA could be explained by incorrect RNA folding.

CONCLUSIONS

We showed that the fluorophore sulforhodamine B binds specifically to the RNA aptamer SRB2m even in the context of total RNA extract. We also showed that sulforhodamine B could bind to the SRB2m aptamer in conjunction with flanking RNA sequences of up to 2 kb. To our knowledge, this is the first evidence for the binding of a small aptamer target to such an elongated aptamer. The in vivo application for the detection of RNA molecules using the SRB2m aptamer and sulforhodamine B system is not practical because sulforhodamine B is known to bind to basic amino acids and is used for the quantification of proteins (25). Therefore, new aptamers for fluorescent dyes need to be selected for the detection of RNAs in living cells. However, the genetic fusion of genes and fluorophore binding aptamers offer a promising tool for the visualization of RNAs in living cells. For in vivo applications, fluorophores can be administered into living cells by microinjection. This method has the drawback

that only singular cells can be monitored. The uptake of fluorescent dyes with the medium seems to be more straightforward, because a whole population of cells could be investigated with this method. Free diffusion of the fluorescent dye into the cell and out of the cell is a prerequisite for the applicability of the dye. Excess of non-aptamer-bound fluorophore needs to be removed from the cytosol to reduce background signals. The selection of other appropriate fluorescent dyes offering the mentioned attributes for in vivo imaging of RNA is in progress.

We thank Stephan Born and Christoph Scheel for help with plasmid construction, and Viswatej Avutu for carefully reading the manuscript.

This work was supported partly by European Commission FP6 funding (LSHC-CT-2004-505785). This publication does not necessarily reflect the views of the European Commission. The Community is not liable for any use that may be made of the information contained herein.

REFERENCES

1. Bashirullah, A., R. L. Cooperstock, and H. D. Lipshitz. 1998. RNA localization in development. *Annu. Rev. Biochem.* 67:335–394.
2. Gonsalvez, G. B., C. R. Urbinati, and R. M. Long. 2005. RNA localization in yeast: moving towards a mechanism. *Biol. Cell.* 97:75–86.
3. Kloc, M., N. R. Zearfoss, and L. D. Etkin. 2002. Mechanisms of subcellular mRNA localization. *Cell.* 108:533–544.
4. Bratu, D. P., B. J. Cha, M. M. Mhlanga, F. R. Kramer, and S. Tyagi. 2003. Visualizing the distribution and transport of mRNAs in living cells. *Proc. Natl. Acad. Sci. USA.* 100:13308–13313.
5. Mhlanga, M. M., D. Y. Vargas, C. W. Fung, F. R. Kramer, and S. Tyagi. 2005. tRNA-linked molecular beacons for imaging mRNAs in the cytoplasm of living cells. *Nucleic Acids Res.* 33:1902–1912.
6. Vargas, D. Y., A. Raj, S. A. Marras, F. R. Kramer, and S. Tyagi. 2005. Mechanism of mRNA transport in the nucleus. *Proc. Natl. Acad. Sci. USA.* 102:17008–17013.
7. Glotzer, J. B., R. Saffrich, M. Glotzer, and A. Ephrussi. 1997. Cytoplasmic flows localize injected oskar RNA in Drosophila oocytes. *Curr. Biol.* 7:326–337.
8. Bullock, S. L., and D. Ish-Horowicz. 2001. Conserved signals and machinery for RNA transport in Drosophila oogenesis and embryogenesis. *Nature.* 414:611–616.
9. Cha, B. J., B. S. Koppetsch, and W. E. Theurkauf. 2001. In vivo analysis of Drosophila bicoid mRNA localization reveals a novel microtubule-dependent axis specification pathway. *Cell.* 106:35–46.
10. Beach, D. L., E. D. Salmon, and K. Bloom. 1999. Localization and anchoring of mRNA in budding yeast. *Curr. Biol.* 9:569–578.
11. Bertrand, E., P. Chartrand, M. Schaefer, S. M. Shenoy, R. H. Singer, et al. 1998. Localization of ASH1 mRNA particles in living yeast. *Mol. Cell.* 2:437–445.
12. Ozawa, T., Y. Natori, M. Sato, and Y. Umezawa. 2007. Imaging dynamics of endogenous mitochondrial RNA in single living cells. *Nat. Methods.* 4:413–419.
13. Valencia-Burton, M., R. M. McCullough, C. R. Cantor, and N. E. Broude. 2007. RNA visualization in live bacterial cells using fluorescent protein complementation. *Nat. Methods.* 4:421–427.
14. Ellington, A. D., and J. W. Szostak. 1990. In vitro selection of RNA molecules that bind specific ligands. *Nature.* 346:818–822.
15. Holeman, L. A., S. L. Robinson, J. W. Szostak, and C. Wilson. 1998. Isolation and characterization of fluorophore-binding RNA aptamers. *Fold. Des.* 3:423–431.
16. Schurer, H., A. Buchynskyy, K. Korn, M. Famulok, P. Welzei, et al. 2001. Fluorescence correlation spectroscopy as a new method for the investigation of aptamer/target interactions. *Biol. Chem.* 382:479–481.
17. Guet, C. C., L. Bruneaux, T. L. Min, D. Siegal-Gaskins, I. Figueroa, et al. 2008. Minimally invasive determination of mRNA concentration in single living bacteria. *Nucleic Acids Res.* 36:e73.
18. Zuker, M. 2003. Mfold web server for nucleic acid folding and hybridization prediction. *Nucleic Acids Res.* 31:3406–3415.
19. Mathews, D. H., J. Sabina, M. Zuker, and D. H. Turner. 1999. Expanded sequence dependence of thermodynamic parameters improves prediction of RNA secondary structure. *J. Mol. Biol.* 288:911–940.
20. Magde, D., E. L. Elson, and W. W. Webb. 1974. Fluorescence correlation spectroscopy. II. An experimental realization. *Biopolymers.* 13: 29–61.
21. Haustein, E., and P. Schwille. 2007. Fluorescence correlation spectroscopy: novel variations of an established technique. *Annu. Rev. Biophys. Biomol. Struct.* 36:151–169.
22. Weisshart, K., V. Jungel, and S. J. Briddon. 2004. The LSM 510 META-ConfoCor 2 system: an integrated imaging and spectroscopic platform for single-molecule detection. *Curr. Pharm. Biotechnol.* 5:135–154.
23. Fradin, C., D. Zbaida, and M. Elbaum. 2005. Dissociation of nuclear import cargo complexes by the protein Ran: a fluorescence correlation spectroscopy study. *C.R. Biol.* 328:1073–1082.
24. Muller, J. J., T. N. Zalkova, D. Zirwer, R. Misselwitz, K. Gast, et al. 1986. Comparison of the structure of ribosomal 5S RNA from *E. coli* and from rat liver using X-ray scattering and dynamic light scattering. *Eur. Biophys. J.* 13:301–307.
25. Vichai, V., and K. Kirtikara. 2006. Sulforhodamine B colorimetric assay for cytotoxicity screening. *Nat. Protocols.* 1:1112–1116.